Vol. (1), No (3), July- September 2024 DOI: 10.21608/MERMJ.2025.349548.1021

Synthesis, Characterization and Antibacterial Activity of a New Ciprofloxacin Derivative Loaded Nanoparticles

Shadwa Abdelfattah[1,*], Doaa M. Saleh[2], Ali M. Elshamsy[3], Hamada Hashem[4]

[1]Department of Pharmaceutics, Faculty of Pharmacy, Merit University, Sohag, 82755, Egypt.

[2]Department of Pharmaceutical Chemistry, Faculty of Pharmacy, Ain shams University11566, Cairo, Egypt.

[3]Department of Pharmaceutical Chemistry, Faculty of Pharmacy, Deraya University, Minia, Minia City 61768, Egypt.

[4] Department of Pharmaceutical Chemistry, Faculty of Pharmacy, Sohag University, Sohag 82524, Egypt.

[*] Corresponding author.

ARTICLE INFO

Article history:
Received 2 Januray2025
Accepted 2 February 2025
Available online 6 February 2025

Keywords:
Ciprofloxacin, Nanoparticles, Antibacterial, Molecular Docking.

Abstract

Nanotechnology breakthroughs present intriguing ways to create new materials that can facilitate drug entrance into bacteria, enable penetration into biofilms, and exhibit synergism with their own functional characteristics. One method of slowing the development of antimicrobial resistance is to encapsulate antibacterial drugs in nanomaterial. By increasing the absorption of antimicrobial medications and thereby halting the development of resistant mutations, antibiotic-loaded nanoparticles may lessen antimicrobial resistance. Additionally, antibiotics at the nanoscale may be able to prevent efflux pumps. A New ciprofloxacin derivative 2 was synthesized and characterized. The newly synthesized compound 2 loaded nanoparticles evaluated as antibacterial agents against *Staphylococcus aureus* as Gram-positive bacteria and *Escherichia coli* and *Pseudomonas aeruginosa* as Gram-negative bacteria using ciprofloxacin as reference. The in vitro antibacterial screening revealed the higher potency of compound 2 loaded nanoparticles against Staphylococcus aureus with MIC value of 0.68 µg/mL than parent ciprofloxacin with MIC value of 3.24 µg/mL and lower activity against Escherichia coli and Pseudomonas aeruginosa (MIC range 0.85-1.17, µg/mL) compared to ciprofloxacin (MIC range 0.17-0.23, µg/mL). Molecular docking studies showed that compound 2 loaded nanoparticles exerts an additional significant binding towards topoisomerase II (gyrase) enzyme (PDB: 2XCT) active.

1. Introduction

One of the most urgent problems facing the world today is the emergence of antimicrobial resistance (AMR), and considerable effort has been made to investigate novel and sophisticated medications. However, the emphasis has turned to enhancing the effectiveness of currently available blockbuster

medications due to extensive and hampered regulatory approval. Nanotechnology Has presented intriguing ways to create new materials that can facilitate drug entrance into bacteria, enable penetration into biofilms, and exhibit synergism with their own functional characteristics[1-3]. Because of their high encapsulation, enhanced bioavailability, reduced toxicity, and improved half-life. The therapeutic agent's site-directed targeted delivery, stability, safety and controlled release are all provided by NPs. Additionally, they have stronger antimicrobial properties[4, 5]. One method of slowing the development of antimicrobial resistance is to encapsulate antibacterial drugs in nanomaterial [6]. By increasing the absorption of antimicrobial medications and thereby halting the development of resistant mutations, antibiotic-loaded nanoparticles may lessen antimicrobial resistance. Additionally, antibiotics at the nanoscale may be able to prevent efflux pumps[6, 7]. All bacterial organisms are thought to acquire resistance mechanisms in response to antimicrobials; however, those with higher mutation frequencies are more likely to develop resistance. Naturally, compared to other clinical isolates, *Escherichia coli* strains have 1000 times greater increased mutation frequencies[8]. Cross-resistance to many drug classes and an increased likelihood of antibiotic resistance are linked to *Escherichia coli*-induced urinary tract infections[9]. CIP [1-cyclopropyl- 6fluoro-1,4dihydro- 4oxo-7piperazinyl quinolone- 3carboxylic acid] is a large spectrum fluoroquinolone antibiotic that is widely used to treat a range of bacterial infections[10]. Bacterial resistance towards chemotherapeutic agents represents a big challenge to the health community [11, 12]. Novel antibacterial drugs are desperately needed to fight resistant bacterial strains[13]. Chemically altering current antibiotics and loading them into nanoparticles are appealing ways to reduce AMR and boost antibiotic effectiveness [14-18].

2. Experimental section

2.1. Chemistry

Using pre-coated aluminum plate silica gel 20 cm x 20 cm and 60 mm plates (eluent: methylene chloride 19: methanol 1 V/V), reactions were tracked by TLC. Spots were identified by passing them under a UV lamp set at ′ = 254 nm. Uncorrected melting points were measured using an electrothermal melting point device (Stuart Scientific.Co.). A Shimaduz instrument Spectrophotometer at Sohag University's Faculty of pharmacy records infrared spectra as KBr disks. At Sohag University's Faculty of pharmacy, NMR spectra were recorded using a Bruker AM NMR (400 MHz) spectrometer. All figures pertaining to the acquired NMR data are expressed by ppm. Carbon, hydrogen, and nitrogen elemental microanalyses were carried out at Al-Azhar University's National Center of Mycology and Bioinformatics in Cairo, Egypt.

2.1.1. Using the documented methods, ethyl (4-acetylphenyl) carbamate (intermediate 1) was made [19, 20].

2.1.2. Standard protocol for synthesis of 7-(4-((4-acetylphenyl) carbamoyl)piperazin-1-yl) synthesis 6-fluoro-1-cyclopropyl-dihydroquinoline-4-oxo-1,43-carboxylic acid (compound 2).

For 20 hours, a combination of CIP (4.0 g, 0.012 mol) and carbamate intermediate 1 (2.5 g, 0.012 mol) in 40 mL of xylene was heated at reflux. To obtain the pure product, the preCIPitate has been filtrated off while still hot, cleaned with xylene and then with acetonitrile, and then dried [14]. white powdered form; 4.7 g, 79.66 % yield; melting point: 272-273ºC; 1H-NMR (400 MHz, DMSO-d6). δ = 1.22-1.256 (2H, m, cyclopropyl-H), 1.33-1.35 (2H, m, cyclopropyl-H), 2.6 (3H, s, CH3), 3.46-3.50 (4H, m, piperazinyl-H), 3.76-3.86 (5H, m, piperazinyl-H and cyclopropyl-H), 7.62 (1H, d, J = 8 Hz, H-8), 7.67 (2H, d, J = 8 Hz, Ar-H), 7.88 (2H, d, J = 8 Hz) δ = 8.07, 26.76, 36.35, 44.07, 49.78, 107.07, 107.32, 111.38, 111.61, 118.72, 119.34, 129.67, 139.64, 14.02 [21].

2.2. Preparation of CIP derivative loaded NPs

Because of their exceptional encapsulation efficiency, CIS: TPP proportions of 3:1 were used to manufacture CIP derivative 2 loaded NPS. Plu. was added in concentrations ranging from 0.5 to 4% w/v to the preceding mixture [22, 23]. The ionic gelation process was used to generate CIS/TPP NPs loaded with CIP 1% w/v CIS was dissolved in 1% acetic acid and then sonicated for half an hour [24, 25].

A- Physicochemical-characterization of CIP derivative 2 NPs (Detection of Size, PDI, and Zeta-potential

A Malvern-Autosizer 4800 with a 488 nm uniphase argonion laser (Malvern Instruments, UK) was used to measure size, PDI, and zeta-potential. The dispersion of the particles inside the solution is referred to as PDI. A monodisperse solution is indicated when the Polydispersity Index falls below 0.5. Triplicate manner of each measurement were taken at a 120° angle and 25°C [26].

B- Morphological properties and evaluation of encapsulation efficiency of nanosized CIP derivative 2

TEM was used to analyze the morphological properties of CIS/Plu NPs (Model 100 CX II, Tokyo,Japan).Thermo Scientific's UV-VIS spectrophotometer was used to assess the encapsulation efficacy of nanosized CIP derivative 2[27]. By centrifuging the nanoparticles from an aqueous solution containing unloaded CIP derivative 2 NPs for 60 minutes at 12,000 x g, the encapsulation effectiveness of nanosized CIP derivative 2 was determined. A wavelength of 254 nm was employed to quantify the amount of CIP deivative 2 in the supernatant [28].

C-Storage stability of fluoroquinolone derivative 2 loaded CIS/Plu NPS:

Nanosized CIP derivative 2 was kept at 4˚C For seven days. Following that, physicochemical characteristics were examined to ascertain how storage affected their stability [29].

D- Evaluation of the in-vitro release pattern of nanosized formulations

This experiment was carried out using the best formulations for CIP derivative 2 loaded CIS/Plu NPs that had been created at Plu conc. 3%. Purified nanoparticle dispersions having a molecular weight of 12 kDa were utilized in dialysis bags (Sigma-Aldrich Co., St. Louis, MO). At room temperature, a thermostatic water bath oscillator (Gesell schaftfürLabortechnik mbH, Burg-Wedel, Germany) was used to stir the dialysis bag while it was dipped in 25 mL of PBS. A certain volume of dialysis medium was removed at various times. Using a UV-VIS spectrophotometer, the amount of CIP deriavative 2 released from the dialysis medium was measured at wavelength of 275 nm and 254 for free CIP and CIP derivative 2 loaded NPS, respectively. The subsequently transformed into cumulative release percentages[30]. For analysis of the release kinetics, curve fitting to a variety of kinetic models [31].

2.3. Determination of MIC

Gram positive and negative bacteria were used to assess the new compound loaded NPs' antibacterial effectiveness. The microbiological resource center at Ain Shams University in Cairo, Egypt, supplied reference strains of *E. coli* (ATCC 8738), *P. aeruginosa* (ATCC 10144), and *S. aureus* (ATCC 6537). 20 ml of Mueller Hinton Agar media (MH agar) were added to each sterile petri dish then average was calculated after the inhibitory zones were measured [32, 33].

2.4. Animals

Thirty healthy male wistern albino mice weighing 20 ± 0.1 mg were used in this study. The study was conducted in accordance with the standard operating protocols of the Committee on Animal Care at sohag University, sohag, Egypt. The animals were given unrestricted access to water during their 12-hour fast before the trial started.

2.5. Docking study

After drawing compound in Chem Draw Ultra (version 8), The RCSB Protein Data Bank provided the 3.35 Å resolution image of the bacterial gyrase complex with DNA and CIP (PDB:2XCT) protein (https://www.rcsb.org/) and employed in docking research. The MOE LigX procedure was used to prepare the protein. CIP derivative 2 and parent CIP docked in the binding site using the triangle matcher placement technique. Forcefield was employed for refinement, and the affinity G scoring system was used for scoring. After the resulting docking study poses were inspected visually, the target compounds were evaluated using the poses that had the least binding free energy value and greatest hydrophobic,

hydrogen bonding, and electrostatic interactions within the target binding pocket of protein [33-35].

3. Results and Discussion

3.1. Chemistry

CIP was refluxed with the ester intermediate 1 in xylene to create CIP derivative 2, which was subsequently identified by ^{1}H-NMR, ^{13}C-NMR, mass spectrometry, and elemental analysis as previously documented (Scheme 1) [34, 35].

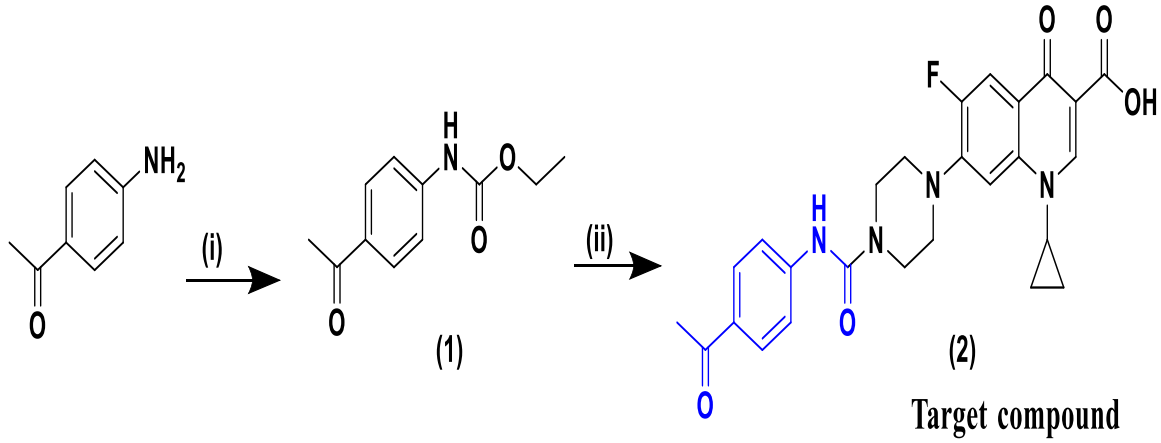

Scheme 1. Synthesis of target compound 2.

Reagents and conditions: (i) Ethyl chloroformate, acetonitrile, pyridine at 0-5 °C; (ii) CIP, Xylene and refluxing for 20 hrs.

A- CIP derivative 2 loaded NPs: physicochemical characterisation (size, PDI, and zeta potential detection)

The ionotropic pregelation method was used to load CIP derivative 2 into CIS:TPP nanoparticles. The ionotropic pregelation is caused by the spontaneous gel formation of chitosan upon interaction with the TPP and the creation of intramolecular and intermolecular linkages between the NH_2 group of chitosan and the PO_4 groups of the TPP. The diameters of the CIP derivative 2-loaded CIS:TPP NPs ranged from 265 to 800 nm. Furthermore, the PDI for nanosized CIP derivative 2 varied between 0.19 and 0.81.

A positive Zeta-potential was observed in the CIS/TPP NPs loaded with CIP derivative 2 (Fig.1:2). CIP loaded NPs showed the lowest size, PDI, and maximum encapsulation efficiency at a CIS/TPP ratio of 3:1; these NPs were chosen for further characterization and CIP loaded CIS/TPP/Pluronic NPs manufacturing. When Plu was added, the size of the NPs decreased, and the final NPs (0.5 to 4% plu) had a size range of 23.2-95 nm for CIS/Plu loaded with CIP. Furthermore, for NPs loaded with CIP derivative 2, the PDI varied between 0.35 and 0.57 (Fig. 1:2).

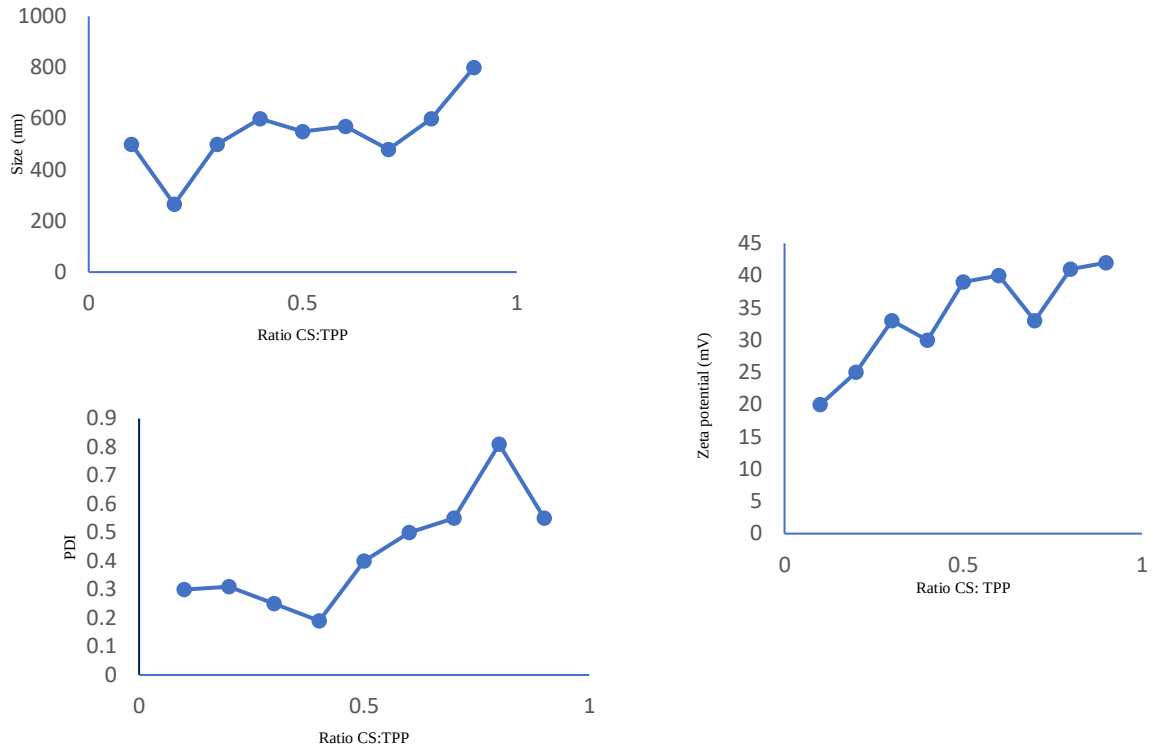

Fig. 1. The impact of the ratio of TPP to CIS on the various characterizations of the nanosized CIP derivative 2 (n = 3, mean ± SD).

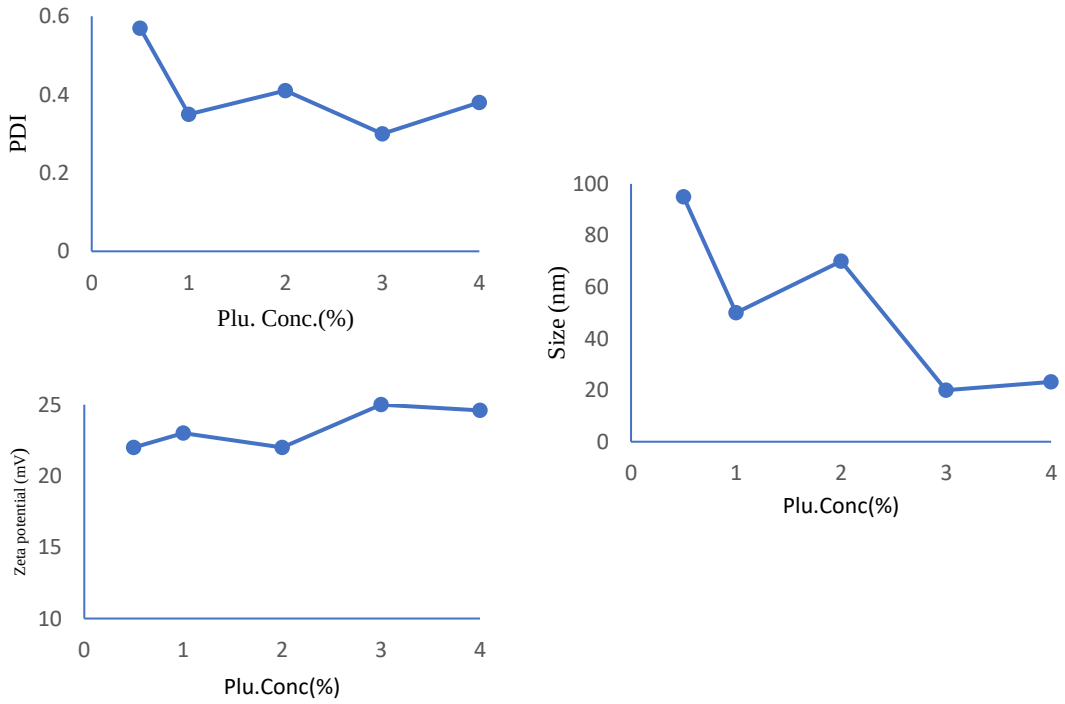

Fig.2. The effect of plu. conc. on the different physicochemical features of nanosized CIP derivative 2 (n = 3, mean ± SD)

B-Morphological properties and Evaluation of encapsulation efficiency of nanosized CIP

Sphericity and nanosized CIP derivative 2 have comparable morphologies (Fig.3). The encapsulation efficiencies of CIP-loaded NPs ranged from 70% to 79.1%. Because the micellar formation/coating effect and the inter and intramolecular crosslinking of chitosan decreased the size and PDI of NPs and resulted in the highest CIP derivative 2 EE% (i.e., 79.1) for 2% w/v and 3% plu. conc. (Table 1:2), these formulations were chosen for further investigation

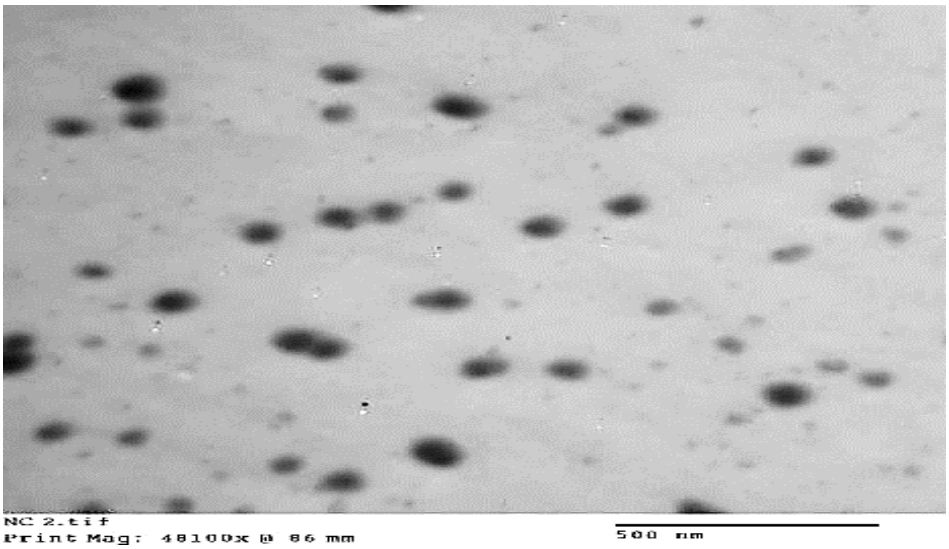

Fig.3. TEM examination of nanosized CIP derivative 2.

CIS:TPP Ratio	(EE%)
1:1	58.8
2:1	58.5
3:1	61.1
4:1	60.8
5:1	59.8
6:1	57.9
7:1	54.7
8:1	50.9
9:1	55.8

Table 1. CIP derivative 2 encapsulated in CIS/TPP NPs had EE% of 1:1 to 9:1 (CIS/TPP) (n = 3, mean ± SD).

Plu. Conc.(%)	EE (%)
0.5	75
1	70
2	76
3	79.1
4	72

Table 2. EE% of CIS/Plu NPs encapsulated CIP derivative 2 at Conc. (0.5-4%) (n =3, mean ± SD).

C-Testing the stability of CIP derivative 2 loaded CIS/Plu nanoparticles:

-CIS/Plu NPs loaded with CIP derivative 2: stability of storage CIS/Plu nanoparticles loaded with CIP derivative 2 showed a little increase in size and PDI after seven days of liquid incubation; they expanded from 47 to 220.5 nm and from 0.31 to 0.65, respectively. Nevertheless, the nanoparticles' zeta potential remained unchanged (Fig. 4).

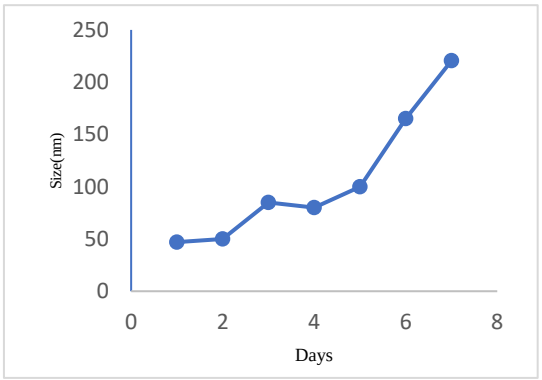

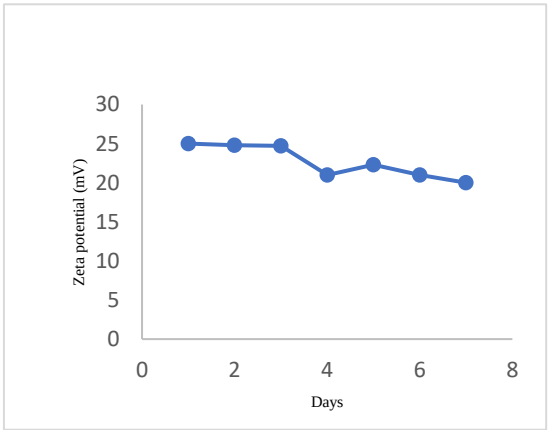

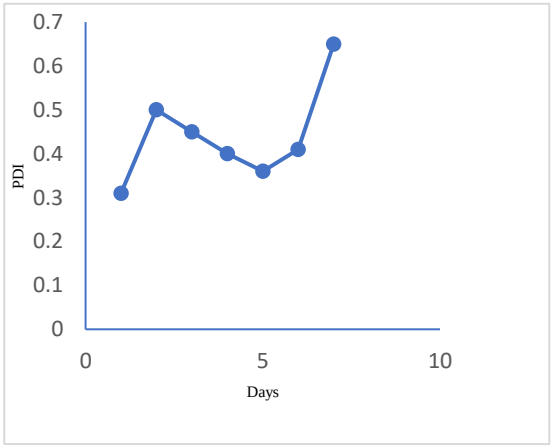

Fig. 4. Effect of storage time on the different physicochemical characteristics of nanosized CIP derivative 2 (n = 3, mean ± SD).

D- Evaluation of the in-vitro release pattern of nanosized formulations

CIP derivative 2's cumulative release pattern in vitro was investigated using both free drug solution and nanosized formulations produced at Plu conc. (3-2% w/v). The CIP release pattern from the free medication solution was almost finished in two to four hours, and no further significant release was seen. An early eruption of the free drug is followed by a persistent release pattern until peak release, which matches the release profile of free CIP derivative 2 from nanosized CIP (Fig.5). The release of CIP derivative 2 from CIS/Plu nanoparticles was regulated by the diffusion process as it was discovered that the release of the nanoparticle fit the Higuchi and Korsmeyer-Peppa models quite well. These formulations are consistent with a fickian diffusion release mechanism since all of the exponent data points were less than 0.45 (Table 3). We used the kinetic models with the highest correlation coefficient value (R^2) to model drug release from CIS/Plu-NPs.

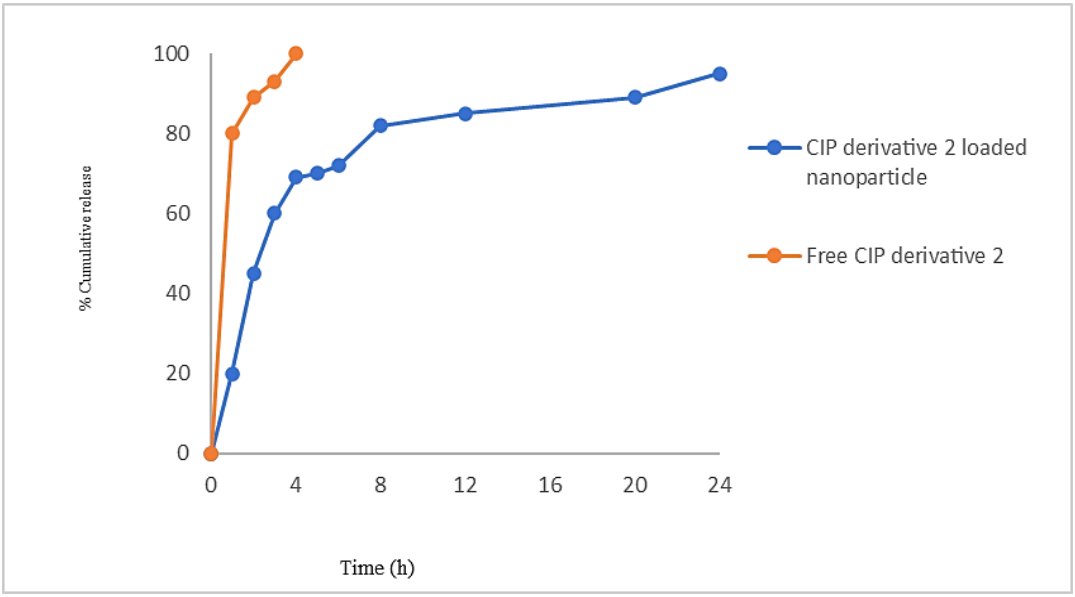

Fig. 5. Drug release (In vitro) pattern of free CIP, and from nanosized CIP in PBS at 37± 0.5° C (n = 3, mean ± SD).

Formulation	Correlation coefficient (R^2)			
	Zero-order	First-order	Higuchi-model	Korsemeyer-Peppas model
CIP-loaded CIS/Plu NPS	0.787	0.843	0.866	0.902

Table 3. Analysis of the kinetics of CIP derivative 2 release from CIS/Plu NPs.

3.3. Screening of antibacterial activities.

Using the conventional agar diffusion method, the antimicrobial properties of compound 2 loaded NPs were assessed in vitro against *S.aureus* (ATCC 6538), *P. aeruginosa* (ATCC 10145), and *E.coli* (ATCC 8739) [36]. CIP served as the reference medication for Compound 2's testing. (Table 4) lists the antimicrobial screening results. Compound 2 loaded nanoparticles displayed a greater activity against Gram-positive organisms *S. aureus* with a MIC value of 0.68µg/mL than parent CIP, which had a MIC value of 3.24 µg/ml. according to the MICs provided in (Table 4). As opposed to free CIP (MIC range 0.17-0.23, µg/mL), compound 2 exhibits less action than CIP against gram-negative strains of *P.aeruginosa* and *E. coli* (MIC range 0.58-1.17, µg/mL).

Compound	**MIC (µg/mL)**		
	Gram-positive	**Gram-negative**	
	S. aureus	***E. coli***	***P.aeruginosa***
Nanosized Compound 2	0.68	0.58	1.17
Free CIP	3.24	0.17	0.23

Table 4: The MICs of antimicrobial activities of the nanosized compound 2 and free CIP (µg/mL).

3.4. In-vivo research of nano-therapeutic compound and free drug loaded carbapol gel on animal model

The treatment model was processed to investigate the wound healing effects of synthesized CIP derivative 2 loade NPs and free CIP both loaded in carbapol gel. The findings showed a 30% improvement in wound healing compared to the control group. To remove skin infection. Compared to the untreated control group, it has been found that new derivative 2 CIP NPs based nano-therapeutics effectively eradicate S.aureus and p.aeuroginosa from infected skin and enhance healing. H&E was used for microscopic analysis of skin to monitor wound healing in three different groups as showen in (Fig.6,7).

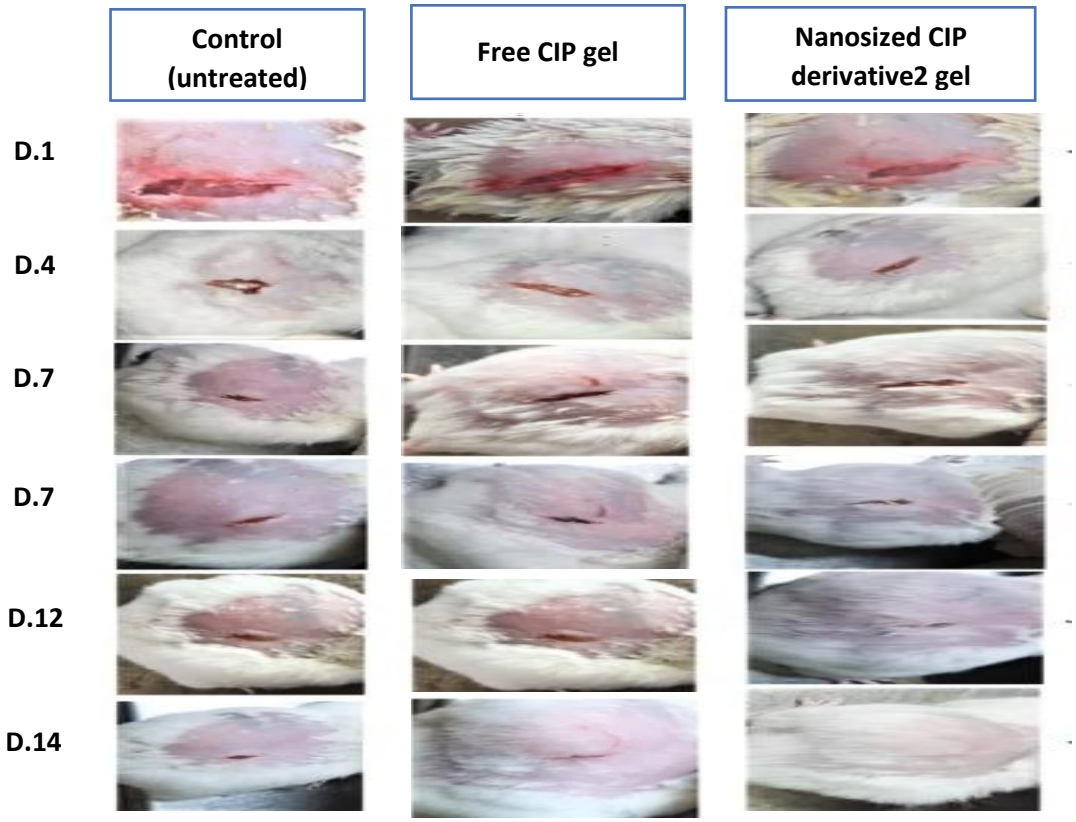

Fig.6. Healing process of wounds in mice model treated with free CIP drug loaded gel and synthesized CIP derivative 2 NPs-based nano-drug system loaded gel.

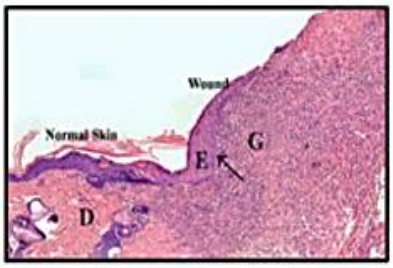

Fig.(A) (group Ⅰ (control) on day 7 post-wounding showing the wound and the nearby normal skin. Partial re-epithelialization (arrow) with newly formed epidermis (E) covering part of the wound area is seen with the underlying granulation tissue (G). Dermis (D) of nearby normal skin is seen A): A photomicrograph of a section of a mice's skin of

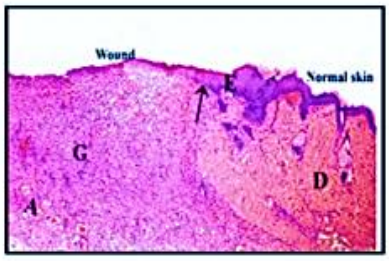

Fig. (B): A photomicrograph of a section of a mice's skin of group II (free CIP treated group) on day 7 post wounding showing the wound and adjacent normal skin. The epidermis (E) at the wound edge is apparently thickened and is creeping to cover part of the wound area (start of re-epithelialization) (arrow). Granulation tissue (G) is seen with an area of angiogenesis (A). Dermis (D) of nearby normal skin is seen.

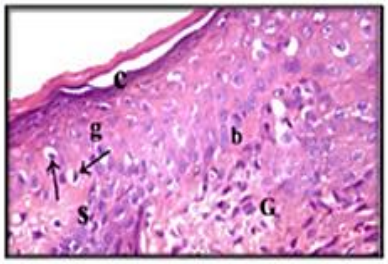

Fig. (C): A photomicrograph of a section of a mice's skin of group III (CIP derivative 2 treated group) on day 7 post-wounding showing the newly formed epidermis with well arranged layers; stratum basal (b), stratum spinosum (s), stratum granulosm (g) and stratum cornum (c). Notice some keratinocytes with pyknotic nuclei (arrow). The underlying granulation tissue (G) is seen

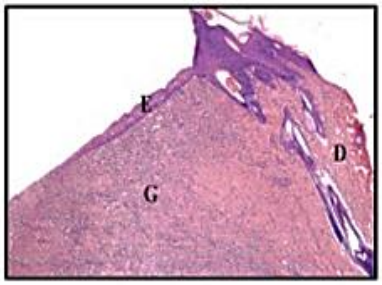

Fig. (D): A photomicrograph of a section of a mice's skin of group Ⅰ (control) on day 14 post-wounding showing incomplete re-epithelialization of the wound area with the newly formed epidermis (E). Note the underlying granulation tissue with numerous blood vessels (G). (D) = dermis of the nearby normal skin.

Fig. (E): A photomicrograph of a section of a mice's skin of group II (free CIP treated group) on day 14 post wounding showing that the wound area is partially covered by epidermis (E) (incomplete re-epithelialization).Note the underlying granulation tissue with numerous blood vessels(G).(D) = dermis of the nearby normal skin.

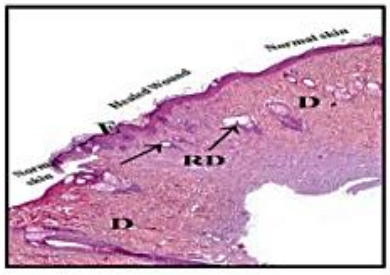

Fig. (F): A photomicrograph of a section of a mice's skin of group III (CIP derivative 2 treated group) on day 14 post-wounding showing that the wound area is completely covered by newly formed epidermis (complete re epithelialization).The underlying regenerated dermis (RD) containing sebaceous glands (arrow) is seen. Dermis (D) of nearby normal skin is also seen on both sides of the wound.

Fig.7. Histological plate of experimental mice skin at 400X magnification power stained with H&E.

3.5. Docking studies

Using MOE software, molecular docking investigations of compound 2 were conducted to look into potential interactions with the important amino acids in the gyrase enzyme's active site. The gyrase enzyme's 3D structure (PDB: 2XCT) was obtained from PDB. The activity of CIP and nanosized compound 2 was explained by their capacity to interact with the crystalline framework of the gyrase protein. (Table 5) lists the binding free energy from the main docked positions. The findings demonstrated that nanosized compound 2 forms an additional hydrogen bond with Lys1066 amino acid and hydrophobic contacts with the gyrase enzyme's active site (ID: 2XCT) (Fig. 8-9).

Compound	Energy score (Kcal/mole)
Nanosized compound 2	-12.8077
Free CIP	-8.7725

Table 5: The binding free energies of nanosized compounds 2 and CIP with topoisomerase II (gyrase) enzyme (PDB: 2XCT) active site.

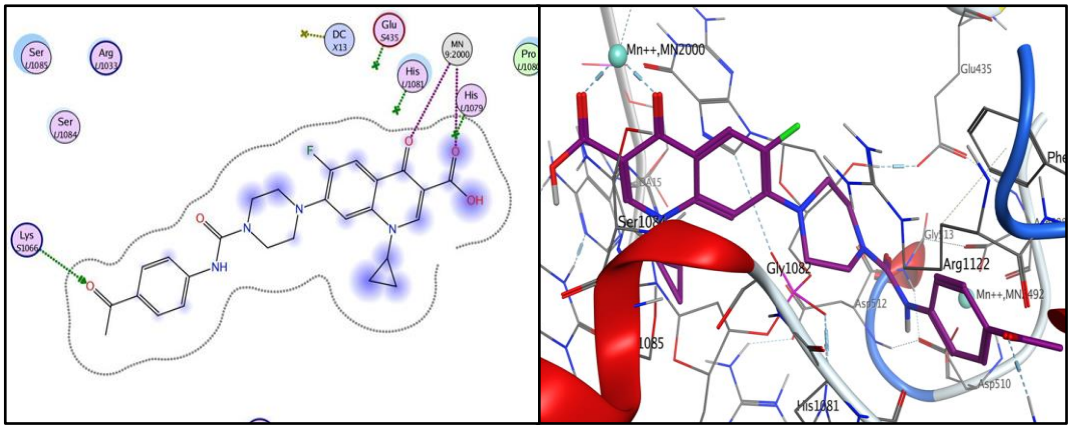

Fig. 8. 2D and 3D binding interactions of CIP within 2XCT active site.

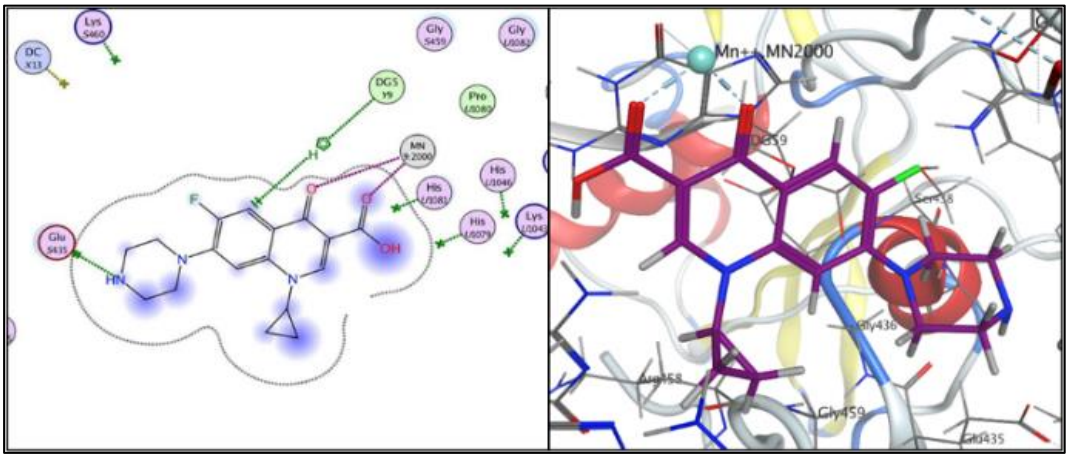

Fig. 9. 2D and 3D binding interactions of nanosized compound 2 within 2XCTactive site.

4. Conclusions

The antibacterial activity of a novel CIP analogue against both Gram-positive as well as Gram-negative bacteria was evaluated after it was synthesized, evaluated using a variety of spectroscopic techniques, and loaded into nanoparticles. Given that the N-4-piperazinyl substitution of CIP increases activity against gram-positive strains, antibacterial activity testing revealed that the newly synthesized CIP derivative 2 has stronger activity against Gram-positive bacteria and less activity against Gram-negative bacteria than its parent CIP. Docking studies show that compound 2 creates an extra bindind hydrogen bond with Lys1066, as well as hydrophobic contacts with the active site of the gyrase enzyme (PDB:2XCT). NPs encapsulation is an alternate strategy for addressing the inadequate absorption and emergence of resistance to conventional antibiotics. NPs increases therapeutic efficacy by enhancing local medication concentration and intracellular bioavailability. This study suggests that a novel antibiotic derivative could be rendered more effective and hence prevent the development of resistance by encasing it in a nano particles matrix. CIP derivative 2 was loaded into CIS/Plu nanoparticles via micellar formation and ionic gelation. The effects of both free and nanosized antibiotic compounds were assessed using MIC. Using innovative derivative antibiotics at the nanoscale may be one of the most promising new ways to treat infections, according to our research, because it can help prevent bacteria from developing resistance mutations.

Abbreviations

CIP: ciprofloxacin.

CIS: Chitosan.

TPP : sodium tripolyphosphate.

P. aeruginosa: pseudomonas aeruginosa.

S.aureus: staphylococcus aureus.

NPs: Nanoparticles.

E.Coli: Escherichia coli.

δ: Delta.

SD : Standard deviation.

TEM : Transmission electron microscopy.

EE%: Entrapment efficiency.

PDI : polydispersity index.

Plu : Pluronic® F-127

Conc : Concentration.

MIC : Minimum inhibitory concentrations.

PBS : Phosphate buffered saline.

Fig : Figure.

CFU : Colony forming unit.

H&E : Hematoxylin and eosin.

D. : Day.

MOE : Molecular operating environment.

References

1. Livermore, D.M., Discovery research: the scientific challenge of finding new antibiotics. J Antimicrob Chemother, 2011. 66(9): p. 1941-4.
2. Vassallo, A., et al., Nanoparticulate antibiotic systems as antibacterial agents and antibiotic delivery platforms to fight infection; Biomedicines s. 2020. 2020(1): p. 6905631.
3. Ghanbarimasir, Z., et al., Design, synthesis, biological assessment and molecular docking studies of new 2-aminoimidazole-quinoxaline hybrids as potential anticancer agents. Spectrochim Acta A Mol Biomol Spectrosc, 2018. 194: p. 21-35.
4. Chen, K.-J., et al., Recent advances in prodrug-based nanoparticle therapeutics. European Journal of Pharmaceutics and Biopharmaceutics, 2021. 165: p. 219-243.
5. Grewal, A.K. and R.K. Salar, Chitosan nanoparticle delivery systems: An effective approach to enhancing efficacy and safety of anticancer drugs. Nano TransMed, 2024. 3: p. 100040.

6. Hetta, H.F., et al., Nanotechnology as a Promising Approach to Combat Multidrug Resistant Bacteria: A Comprehensive Review and Future Perspectives. Biomedicines, 2023. 11(2). p. 200-243.
7. Aflakian, F., et al., Nanoparticles-based therapeutics for the management of bacterial infections: A special emphasis on FDA approved products and clinical trials. European Journal of Pharmaceutical Sciences, 2023. 188: p. 106515.
8. Qadri, F., et al., Enterotoxigenic Escherichia coli in developing countries: epidemiology, microbiology, clinical features, treatment, and prevention. Clin Microbiol Rev, 2005. 18(3): p. 465-83.
9. Niranjan, V. and A. Malini, Antimicrobial resistance pattern in Escherichia coli causing urinary tract infection among inpatients. Indian J Med Res, 2014. 139(6): p. 945-8.
10. Herizchi, R., et al., Current methods for synthesis of gold nanoparticles. 2016. 44(2): p. 596-602.
11. Ahmed, S.K., et al., Antimicrobial resistance: Impacts, challenges, and future prospects. Journal of Medicine, Surgery, and Public Health, 2024. 2: p. 100081.
12. Chinemerem Nwobodo, D., et al., Antibiotic resistance: The challenges and some emerging strategies for tackling a global menace. J Clin Lab Anal, 2022. 36(9): p. 24655.
13. Belete, T.M., Novel targets to develop new antibacterial agents and novel alternatives to antibacterial agents. Human Microbiome Journal, 2019. 11: p. 100052.
14. Hussain, S., et al., Antibiotic-loaded nanoparticles targeted to the site of infection enhance antibacterial efficacy. Nat Biomed Eng, 2018. 2(2): p. 95-103.
15. Raza, A., et al., Solid nanoparticles for oral antimicrobial drug delivery: a review. Drug Discovery Today, 2019. 24(3): p. 858-866.
16. Zhang, G.-F., et al., Ciprofloxacin derivatives and their antibacterial activities. European Journal of Medicinal Chemistry, 2018. 146: p. 599-612.
17. Levine, C., H. Hiasa, and K.J. Marians, DNA gyrase and topoisomerase IV: biochemical activities, physiological roles during chromosome replication, and drug sensitivities. Biochimica et Biophysica Acta (BBA) - Gene Structure and Expression, 1998. 1400(1): p. 29-43.
18. Hooper, D.C. and G.A. Jacoby, Topoisomerase Inhibitors: Fluoroquinolone Mechanisms of Action and Resistance. Cold Spring Harb Perspect Med, 2016. 6(9). p. 145-154.
19. Abdel-Latif, E., M. Mohammed Fahad, and M. Ismail, Synthesis of N -aryl 2-chloroacetamides and their chemical reactivity towards various types of nucleophiles. Synthetic Communications, 2019. 50: p. 1-26.
20. Nguyen, T., et al., Synthesis and Pharmacological Evaluation of 1-Phenyl-3-Thiophenylurea Derivatives as Cannabinoid Type-1 Receptor Allosteric Modulators. J Med Chem, 2019. 62(21): p. 9806-9823.
21. Aziz, H.A., et al., Thiazolidine-2,4-dione-linked ciprofloxacin derivatives with broad-spectrum antibacterial, MRSA and topoisomerase inhibitory activities. Molecular Diversity, 2022. 26(3): p. 1743-1759.
22. Hadiya, S., et al., Levofloxacin-Loaded Nanoparticles Decrease Emergence of Fluoroquinolone Resistance in Escherichia coli. Microbial Drug Resistance, 2018. 24. p. 104-242.
23. Wiggers, H.A., et al., Polyethylene Glycol-Stabilized Zein Nanoparticles Containing Gallic Acid. Food Technol Biotechnol, 2022. 60(2): p. 145-154.
24. Yan, J., et al., Preparation of Puerarin Chitosan Oral Nanoparticles by Ionic Gelation Method and Its Related Kinetics. Pharmaceutics, 2020. 12(3). p. 145-154
25. Zarzycki, P., M. Bartoszuk, and A. Radziwon-Balicka, Optimization of TLC detection by phosphomolybdic acid staining for robust quantification of cholesterol and bile acids. Jpc-journal of Planar Chromatography-modern Tlc - JPC-J PLANAR CHROMAT-MOD TLC, 2006. 19: p. 52-57.
26. Jiamphun, S. and W. Chaiyana, Enhancing Skin Delivery and Stability of Vanillic and Ferulic Acids in Aqueous Enzymatically Extracted Glutinous Rice Husk by Nanostructured Lipid Carriers. Pharmaceutics, 2023. 15. p. 1145-1154
27. Malatesta, M., Transmission Electron Microscopy as a Powerful Tool to Investigate the Interaction of Nanoparticles with Subcellular Structures. Int J Mol Sci, 2021. 22(23). p. 104-242.
28. Soliman, N.M., et al., Development and Optimization of Ciprofloxacin HCl-Loaded Chitosan Nanoparticles Using Box-Behnken Experimental Design. Molecules, 2022. 27(14). p. 145-354.
29. Rees, V.E., et al., Meropenem Combined with Ciprofloxacin Combats Hypermutable Pseudomonas aeruginosa from Respiratory Infections of Cystic Fibrosis Patients. Antimicrob Agents Chemother, 2018. 62(11). p. 145-154.
30. Merlin, J.P.J. and X. Li, Role of Nanotechnology and Their Perspectives in the Treatment of

Kidney Diseases. Front Genet, 2021. 12: p. 817-974.
31. Omar, A.Z., et al., Synthesis and Antimicrobial Activity Screening of Piperazines Bearing N,N'-Bis(1,3,4-thiadiazole) Moiety as Probable Enoyl-ACP Reductase Inhibitors. Molecules, 2022. 27(12). p. 145-154.
32. Bonev, B., J. Hooper, and J. Parisot, Principles of assessing bacterial susceptibility to antibiotics using the agar diffusion method. J Antimicrob Chemother, 2008. 61(6): p. 1295-301.
33. Nawaz, A., et al., Ciprofloxacin-Loaded Gold Nanoparticles against Antimicrobial Resistance: An In Vivo Assessment. 2021. 11(11): p. 3152.
34. Mohammed, H.H.H., et al., Novel urea linked ciprofloxacin-chalcone hybrids having antiproliferative topoisomerases I/II inhibitory activities and caspases-mediated apoptosis. Bioorganic Chemistry, 2021. 106: p. 104-422.

Corresponding author: Shadwa Abdelfattah Ahmed Mousa

Department of Pharmaceutics, Faculty of Pharmacy,

Merit University Egypt (MUE), Sohag, Egypt.

E-mail: shadwaabdelfattah @gmail.com

Phone: 01029493920